

# Weierstraß-Institut für Angewandte Analysis und Stochastik

im Forschungsverbund Berlin e.V.

Preprint

ISSN 0946 – 8633

## Dynamics of a surface-tension-gradient-driven liquid film rising from a reservoir onto a substrate

Peter L. Evans<sup>1</sup> and Andreas Münch<sup>2</sup>

submitted: February 23, 2005

<sup>1</sup> Humboldt University of Berlin, Institute of Mathematics, D-10099 Berlin.  
[pevans@mathematik.hu-berlin.de](mailto:pevans@mathematik.hu-berlin.de)

<sup>2</sup> Weierstrass Institute for Applied Analysis and Stochastics (WIAS),  
Mohrenstraße 39, D-10117 Berlin. [muench@mathematik.hu-berlin.de](mailto:muench@mathematik.hu-berlin.de)

No. 1009  
Berlin 2005



---

Supported by the DFG Research Centre MATHEON (Project C10) in Berlin..

Edited by  
Weierstraß-Institut für Angewandte Analysis und Stochastik (WIAS)  
Mohrenstraße 39  
10117 Berlin  
Germany

Fax: + 49 30 2044975  
E-Mail: [preprint@wias-berlin.de](mailto:preprint@wias-berlin.de)  
World Wide Web: <http://www.wias-berlin.de/>

## Abstract

On a tilted heated substrate, surface tension gradients can draw liquid up out of a reservoir. The resulting film thickness profile is controlled by the tilt of the substrate, the imposed temperature gradient, and the thickness of a postulated thin precursor layer. The evolution of this film in time is studied using a lubrication model. A number of distinct behaviours are possible as the substrate tilt angle and other parameters are varied. Recent results for the multiple stationary profiles possible near the meniscus are used, and the interaction of these profiles with the advancing front is examined. It is shown how to systematically determine the evolution of the entire film profile from the meniscus to the apparent contact line. This allows a categorisation of the range of behaviours for a transversely-uniform profile, in a two-dimensional parameter space. In addition to capillary fronts, and double shock structures, a new combination of a Type I meniscus with a rarefaction fan, and either an undercompressive or a classical wave at the advancing front, that arises for certain ranges of large substrate tilt and precursor thickness is described.

## 1 Introduction

In this paper we consider the time-dependent behaviour of a thin liquid film on a tilted heated substrate. Such a film is produced when a temperature difference is imposed along a substrate with one end immersed into a reservoir containing a liquid such as silicone oil, giving rise to a surface tension gradient. The resulting surface shear stress drags liquid up from the reservoir, while gravitational forces act to return liquid to the reservoir. This may give rise to a film of liquid which climbs up the substrate. The evolution of the film above the reservoir has received considerable attention in recent years [9, 10, 14]. An understanding of thin-film flows driven by surface tension gradients is of importance, for instance in “Marangoni drying” [7], and controlling flows in microfluidic applications [5].

Experiments (e.g.[12, 13]) reveal that the film tends to advance with a steep front at a contact line, where the liquid-air interface meets the substrate. Previous studies have considered the film behaviour in the vicinity of the meniscus, and at the advancing front, independently of each other. The advancing front can be a simple compressive one, or an undercompressive shock as part of a double wave structure [2, 9]. Furthermore, it is known that at the meniscus, multiple film profiles are possible. For a fixed combination of substrate inclination and shear stress, the meniscus can settle into either of two different profiles [11]. In this paper we determine which meniscus profiles are linked with which travelling wave profiles, and how

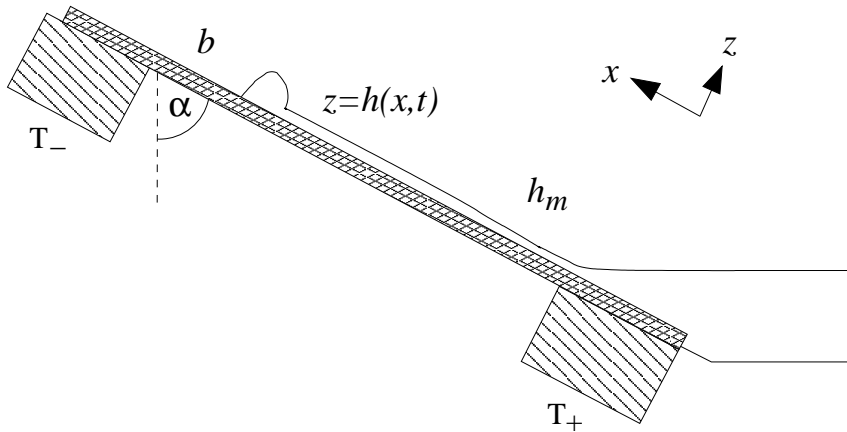


Figure 1: The thin film on a heated tilted substrate rises from a meniscus. Two heaters hold the temperature at the ends of the substrate at temperatures  $T_+ > T_-$ . The resulting Marangoni shear stress drives a thin liquid film of thickness  $h(x, t)$  up the substrate. At the front, the film advances over a thin precursor layer of thickness  $b$  (not shown).

this link occurs, i.e., which are selected. In the sense that this is a composite description, this work is in the spirit of earlier work by Hocking [6] on the connection between a moving contact line and the meniscus, during withdrawal of a moving substrate, which is closely related to the present work. The picture that emerges here for the Marangoni-driven film is, however, more complicated, since we have to include the additional possibility arising from structures involving non-classical waves in our investigation.

As in our earlier work [11], we consider the arrangement shown in Figure 1. The substrate is held at an angle  $\alpha$  measured from the vertical, and it is heated so as to impose a uniform temperature gradient  $(dT/dx) = \gamma < 0$  along the substrate. The film surface tension is  $\sigma$  at some reference temperature, and  $\sigma_T = (d\sigma/dT) < 0$  is the sensitivity of the surface tension to temperature changes. The shear stress is then  $\tau = \gamma\sigma_T$ . The film density is  $\rho$ , and  $g$  is the acceleration due to gravity. We begin in Section 2 with a statement of the equations governing the film evolution, and with brief reviews of the evolution of the film at the meniscus and advancing front, considered individually. The dimensionless parameter  $D$  was introduced by Bertozzi *et al.* [2]. It is a measure of both the substrate angle  $\alpha$  and the strength of the surface shear stress driving the flow. Thus

$$D = \left( \frac{3\delta}{\cos^2 \alpha} \right)^{2/3} \sin \alpha, \quad \text{where } \delta = \frac{\tau}{2\sqrt{\sigma\rho g}}. \quad (1)$$

For large inclinations (and fixed shear stress) the parameter  $D$  is relatively large, and in this case the normal component of gravity is important. A distinct separation between the meniscus and a structure at the advancing front occurs in some circumstances. By considering the possible interaction between these structures, we describe what structures can arise, and the connections between them, in Section 3.

The combined picture we present is confirmed by dynamical simulations. The large  $D$  limit is considered in Section 4. In this case we find that the film can no longer be thought of as separate meniscus and front structures; instead the film smoothly varies from one to the other without a flat region. The result of our investigations in Sections 3 and 4 is a coherent picture of the film behaviour as  $D$ , and the thickness of a presumed precursor layer, are varied, which we present Section 5. Finally Section 6 summarises our work.

## 2 Preliminaries

### 2.1 Formulation

We denote the time-dependent film thickness profile by  $h(x, t)$ , where  $x$  measures distance up the substrate and  $t$  is time. Using ideas from singular perturbation theory, an evolution equation governing  $h(x, t)$  may be obtained [9]. This governing equation is

$$h_t + \Omega_x(h^2 - h^3)_x = -(h^3 \kappa_x)_x + D(h^3 h_x)_x \quad (2)$$

where  $\kappa = h_{xx}(1 + \epsilon^2 h_x)^{-3/2}$  is the nonlinear expression for the curvature of the free surface. Here  $\Omega$  is a dimensionless temperature profile for which  $\Omega_x = 1$  except near the heaters, where  $\Omega$  becomes constant, cutting off surface tension gradients there. Equation (2) is obtained by scaling  $h$ ,  $x$ , and  $t$  by

$$H = \frac{3\tau}{2\rho g \cos \alpha}, \quad L = \left( \frac{3\sigma\tau}{2\rho^2 g^2 \cos^2 \alpha} \right)^{1/3}, \quad \tau = 2\mu \left( \frac{4\sigma\rho g \cos \alpha}{9\tau^5} \right)^{1/3}$$

respectively. The terms in  $h^2$  and  $h^3$  on the left-hand side of (2) account for the competing effects of the imposed shear stress and drainage due to the component of gravity parallel to the substrate. The first term on the right-hand side is due to surface tension, which is supposed to not differ appreciably from its reference value, except inasmuch as it provides the driving shear stress. The second arises from the levelling effect of the component of gravity normal to the substrate. It is useful to define the flux function,  $f(h) = h^2 - h^3$ , which represents the flux of liquid up the substrate in the absence of the second- and fourth-order smoothing terms in (2).

An appropriate boundary condition at the meniscus is that the film profile flattens out to meet the undisturbed reservoir, so

$$h \sim -x/D \quad \text{as } x \rightarrow -\infty. \quad (3)$$

To avoid the singularity associated with a moving contact line, we adopt a precursor model so

$$h \rightarrow b \quad \text{as } x \rightarrow \infty. \quad (4)$$

and define the apparent contact line to be the point where the film thickness first becomes approximately  $b$ .

As explained in our earlier work [11], when  $\epsilon = H/L = (9\delta^2/\cos\alpha)^{1/3} \ll 1$ , it is appropriate to replace  $\kappa$  by the approximate expression  $h_{xx}$  in the thin film region away from the reservoir. In addition, when  $\epsilon \ll D$  it follows that  $\epsilon|h_x| \ll 1$  in the vicinity of the reservoir, and approximating  $\kappa$  by  $h_{xx}$  is also appropriate there. We set  $\Omega_x \equiv 1$ , requiring that as  $\alpha$  is increased the position of the heater is moved further into the reservoir. In this way a uniform temperature gradient, and hence uniform shear stress, is imposed. Equation (2) then reduces to

$$h_t + (h^2 - h^3)_x = -(h^3 h_{xxx})_x + D(h^3 h_x)_x. \quad (5)$$

We are concerned with the behaviour of solutions of (5) subject to (3) and (4). Solutions of (3-5) are potentially influenced by just two parameters,  $D$  defined by (1) above, and the precursor layer thickness,  $b$ . A particular combination of these parameters determines the structure of the climbing film. In the following sections, we enumerate and describe the possible film structures.

Solutions of (5) typically have two distinct parts, a meniscus and a wave structure consisting of one or two advancing waves. Near the reservoir the meniscus part settles into an equilibrium solution with thickness approaching some value  $h_m$ . At the moving apparent contact line is a travelling wave which we refer to as the ‘‘advancing front’’. Behind it may be additional waves, which together with the advancing front make up the moving wave structure.

A good guide to the possible behaviour of the complete film comes from considering what happens considering the two parts independently. In the remainder of this section, we first describe the waves near the contact line. Here the resulting wave structure is determined by a left thickness  $h_w$ , together with  $D$  and  $b$ . We then (in Section 2.3) summarise what limiting meniscus thicknesses  $h_m$  are possible for a given  $D$ .

## 2.2 Advancing front behaviour

A previous study [8] presented a family of travelling wave profiles for the advancing front. These were produced by varying  $D$ , with a fixed choice for the precursor thickness  $b$ . They included compressive waves, and double wave structures [1, 2, 8]. The compressive waves have a characteristic capillary ridge connecting a left state  $h_w$  to the precursor layer with thickness  $b$ . One double wave structure (a ‘‘double shock structure’’) consists of a leading wave, which is undercompressive and has a left state  $h_{uc}$  and right state  $b$ , and a trailing wave which is compressive, with left state  $h_w < h_{uc}$  and right state  $h_{uc}$ . Another structure is formed by the combination of a rarefaction wave, in which the film thickness smoothly decreases from  $h_w > h_{uc}$  until reaching  $h_{uc}$ , and an undercompressive leading wave. The two waves of the double wave structure are separated by a plateau of thickness  $h_{uc}$  which depends on both  $b$  and  $D$ . They both have a positive speed, and so move up the substrate over time. However, since the undercompressive wave moves faster than the compressive wave or the rarefaction fan, the width of the plateau grows over time.

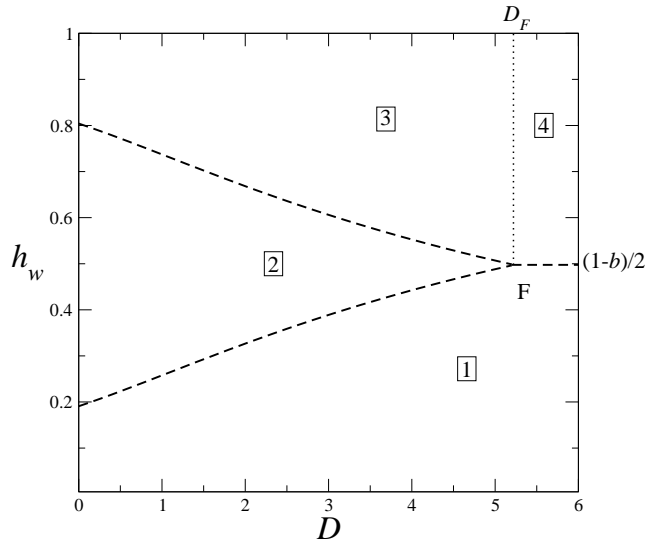


Figure 2: The front wedge diagram for  $b = 0.005$  showing the four possible types of behaviour depending on the left state value  $h_w$  and  $D$ . (The meanings of Regions 1 to 4 are given in the text.)

The results from this earlier study may be summarised in a two-dimensional diagram that displays, for each  $D$ , the values of left states  $h_w$  where the different types of wave or waves connecting this state to the precursor right state exist. In the  $(D, h_w)$  plane, the boundaries between these different ranges essentially form a wedge-like shape, shown in Figure 2 for the precursor thickness  $b = 0.005$ . This shape is defined by the graphs of  $h_{uc}(D, b)$  (at the upper edge) and  $1 - h_{uc} - b$  (lower edge). We refer to this shape as the “front wedge”.

Because  $h_{uc}$  depends on  $b$ , the shape and position of the front wedge on a  $(D, h_w)$  diagram also depends on  $b$ . The apex of the wedge (shown as  $F$  in Figure 2) is located at  $(D_F, (1 - b)/2)$ , where  $D_F$  is itself a monotone decreasing function of  $b$ . The significance of this will become apparent in Section 3. The two sides of the wedge, together with the extension of the wedge’s apex  $\{(D, h) : D > D_F, h = (1 - b)/2\}$ , and the line  $\{(D, h) : D = D_F, h > (1 - b)/2\}$  divide the plane into four regions, labelled 1-4 in the figure. Which wave structure results from a particular  $(D, h_w)$  pair is indicated by the region in which the pair belongs. For relatively small values of  $h_w$ , corresponding to Region 1, a simple compressive wave arises. This wave has a capillary ridge that diminishes as  $D$  increases. Within the wedge (Region 2), one obtains the compressive-undercompressive double shock structure described above. Finally, for large values of  $h_w$ , one obtains double wave structures involving a rarefaction fan; these are either a rarefaction-undercompressive wave when  $D < D_F$  and  $h_w > h_{uc}$  (Region 3), or a rarefaction-shock wave (with a leading generalized Lax-shock), for larger  $D$  (Region 4). To the right of the apex ( $D > D_F$ ) there are no structures involving undercompressive waves: above  $(1 - b)/2$  there is a rarefaction-shock wave combination, while below this line a simple compressive wave occurs.

We have limited the above discussion to values of  $h_w > b$ . In this study, the initial film profiles used (see the Appendix) have thickness  $h \geq b$  everywhere, and so the thickness at later times is never much smaller than  $b$ .

In addition, we have simplified matters by neglecting the presence of a thin region of thicknesses  $h_w$  located around the lower side of the wedge. This exists for a range of  $D$  close to zero, where multiple wave structures that connect  $h_w$  to  $b$  are possible, either one of a number of compressive waves or the double shock structure. This range ends towards the right at a value  $D$  (say  $D_1$ ) below two [8]. Which wave structure is selected in a numerical simulation depends on the initial profile; for monotone initial data connecting  $h_w$  and  $b$ , a single compressive wave with the smallest capillary ridge typically arises [1, 2]. Hence for such initial data and  $D < D_1$ , the range of  $h_w$  for which we get a single compressive front is slightly increased above the lower edge of the wedge.

### 2.3 Meniscus structures

Likewise, in earlier work [11] we demonstrated that two distinct types of behaviour are possible at the meniscus. For a range of positive values of  $D < D_M = 0.8008$ , the film profile where the liquid leaves the reservoir can be matched onto a flat region of constant thickness  $h_m$ , with several possible thicknesses. For this range of  $D$ , a stationary meniscus solution can be found for which  $h_m < 2/3$ , for one special value of  $h_m = h_B(D)$ . We define  $h_T$  to be the larger positive root of  $h^2 - h^3 = f(h_B)$ , so  $h_T > 2/3$ . Then stationary menisci exist when  $h_m$  is  $h_B$ , or is equal to or greater than  $h_T$ . When the film takes the smaller of these two values,  $h_m = h_B(D)$ , its profile, denoted a Type I meniscus solution, monotonically decreases in thickness as it approaches  $h_B$ . When the film takes  $h_m \geq h_T(D)$ , we call this a Type II meniscus solution. Its profile typically has a slight depression or dimple in the meniscus region, and the thickness approaches  $h_m$  by a damped oscillation (when  $D < 0.6964$ ). We call this a Type II meniscus solution. Figure 3 shows the thicknesses  $h_T(D)$  and  $h_B(D)$  for Type I and Type II solutions in an  $(h, D)$  plane. These values merge with  $h = h_T = h_B = 2/3$  when  $D = D_M$ , at the point labelled  $M$  in the figure. For  $D > D_M$ , no Type I meniscus profiles exist, while Type II occur for  $h_m > 2/3$ . We call the structure formed by the graphs of  $h_T(D)$  and  $h_B(D)$  the “meniscus wedge”. Note that this structure does not depend on  $b$ .

When  $h_m$  is near  $h_T(D)$ , and  $D < D_B$ , there are multiple steady Type II solutions which share the same value of  $h_m$  for a given value of  $D$ . Here  $D_B = 0.7142$  is the point where the character of the eigenvalues at the fixed point associated with  $h_B$  change character [11]. The range of thicknesses with multiple Type II solutions is not precisely shown in Figure 3, but is indicated there by the shaded line along  $h_T(D)$ , ending in a solid dot in the figure at  $D = D_B$ . The profiles of four of the multiple Type II menisci are shown in Figure 4 for  $D = 0.322$  and  $h_m = h_T(0.322) \approx 0.8744$ . The question of which, if any, of these are stable to in-plane disturbances then arises. Numerical simulations of the time-dependent PDE (5) revealed that these



are alternately stable and unstable. These simulations were initialised using the Type II profiles computed by a shooting method [11]. The unstable solutions to the ODE do not occur as solutions of the PDE at long times; instead, initial conditions which are close to these evolve toward the stable solutions. In Figure 4 the stable and unstable solutions are shown in solid and dashed lines respectively. This is similar to the situation for the multiple double shock structures described in the previous section.

### 3 Interaction of meniscus and front dynamics

The information summarised in Section 2.2, and encapsulated in the “front wedge” diagram, gives a fairly complete picture on which wave, or combinations of waves, arises near the contact line if, for given  $b$  and  $D$ , the leftmost value of the film thickness is set at some specific value,  $h_w$ . The question of how this value is selected then arises; it is evident that the meniscus plays an important role here. If at long times, when the contact line has travelled far from the reservoir, the meniscus profile approaches a steady state, then the value of  $h_w$  must be equal to an  $h_m$  for which either a Type I or Type II solution exists. This information is found in the “meniscus wedge” diagram in Section 2.3. An overview of the possible combinations of the different types of meniscus and wave structures can be obtained by superimposing the two wedge diagrams. In many cases, this suggests more than just one possible outcome for a given  $D$  and  $b$ . For example, if  $D < D_M$ , wave structures can be found to connect to either a Type I or a whole range of Type II meniscii. However, the only situations which can arise dynamically are those for which the wave part next to the meniscus has a non-negative speed. (If its speed were negative, such a wave part could never emerge from the meniscus.) Rarefaction waves, or parts of rarefaction waves, move with a wave speed given by characteristics, namely  $f'(h)$  where the film thickness is  $h$ . For shock profiles, with left and right states  $h_-$  and  $h_+$  the wave speed  $s$  is given by the Rankine-Hugoniot condition,  $s = (f(h_+) - f(h_-))/(h_+ - h_-)$ .

In this section we use such considerations to determine which meniscus and film profile eventually evolves from monotone initial data representing a thin precursor layer on a substrate is partially immersed into the reservoir, where the meniscus is free of surface tension gradients. The approach outlined above nearly always allows us to single out one possible scenario. The exceptions will be pointed out further below. We then verify our predictions using time-dependent simulations of Equation (5). The initial condition, together with additional details of the simulations are given in Appendix A.

As explained in Section 2.2, the apex of the front wedge at  $D = D_F$  moves towards smaller values of  $D$  as  $b$  is increased. Following Bertozzi *et al.* [2],  $b$  is restricted to be less than  $1/3$ . Depending on  $b$ , the front wedge and meniscus wedge can therefore overlap in four characteristic arrangements, with transitions between these arrangements happening at three critical values of  $b$ . In increasing order of  $b$ , these are as follows:

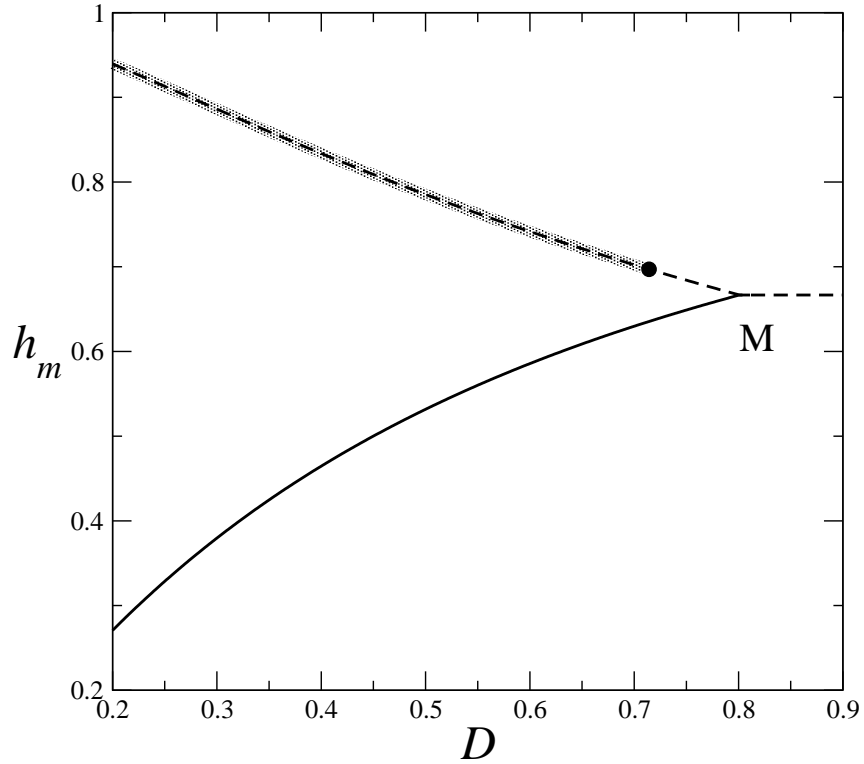


Figure 3: The  $(D, h)$  diagram, showing the meniscus wedge. Lines show the allowable values for the right state of the meniscus,  $h_m$ . For  $D < D_M$ , the meniscus may approach a thickness  $h_m$ , where  $h_m = h_B(D)$  is given by the lower branch, or  $h_m \geq h_T(D)$ , shown in the upper branch. The shaded line indicates the region where multiple Type II menisci are possible. For  $D > D_M$ ,  $h_m \geq 2/3$ .

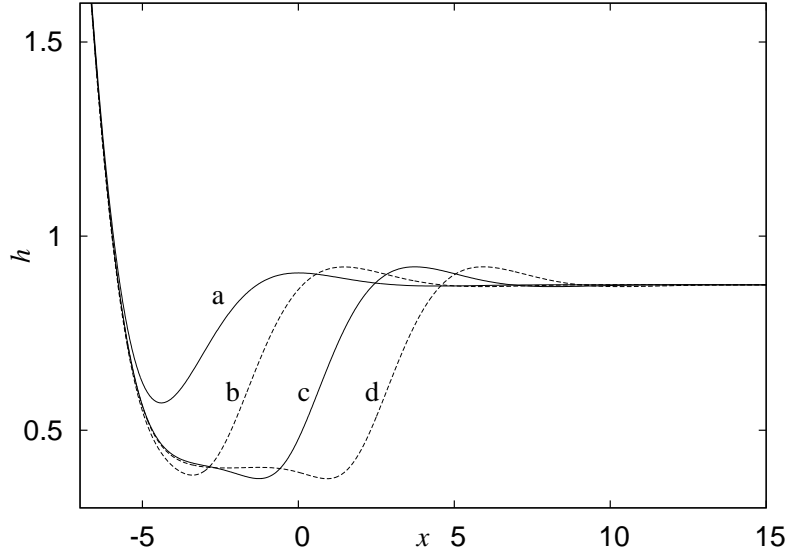


Figure 4: The first four stable (solid lines) and unstable (dashed lines) Type II steady meniscus profiles, for  $D = 0.322$ . Here  $h_m = h_T(0.322) = 0.8744$ , so there is an infinite number of these profiles.

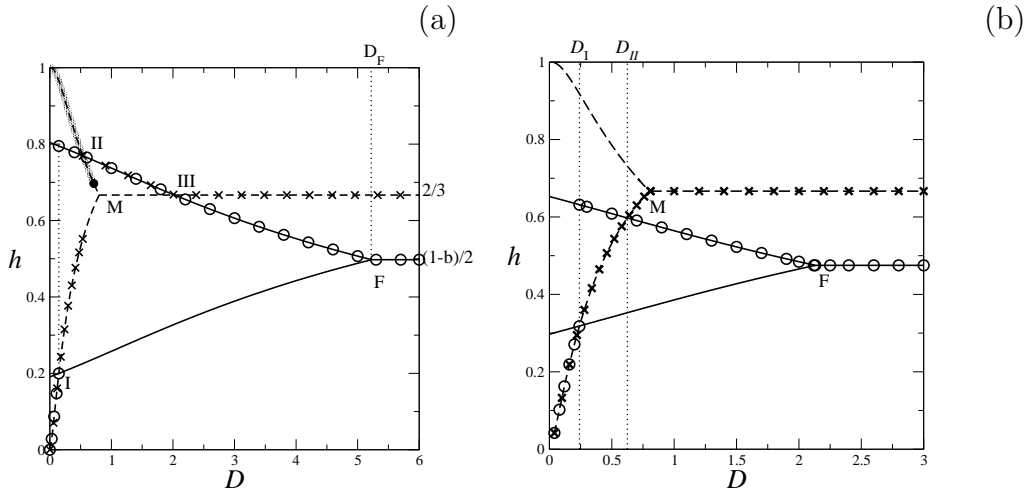


Figure 5: The  $(D, h)$  diagrams, showing the front wedge (solid lines) and meniscus wedge (dashed lines). A line marked with circles indicates the left state  $h_f$  of the advancing front. A line with crosses indicates the right state of the meniscus,  $h_m$ . When these lines coincide, there is a flat film region directly connecting the meniscus to the advancing front. (a) shows Arrangement A, when  $b = 0.005$ ; (b) shows Arrangement B for  $b = 0.05$ . In (b), a new profile featuring a Type I meniscus connected to a rarefaction fan becomes possible for  $D$  between  $D_{II}$  and  $D_M$ .

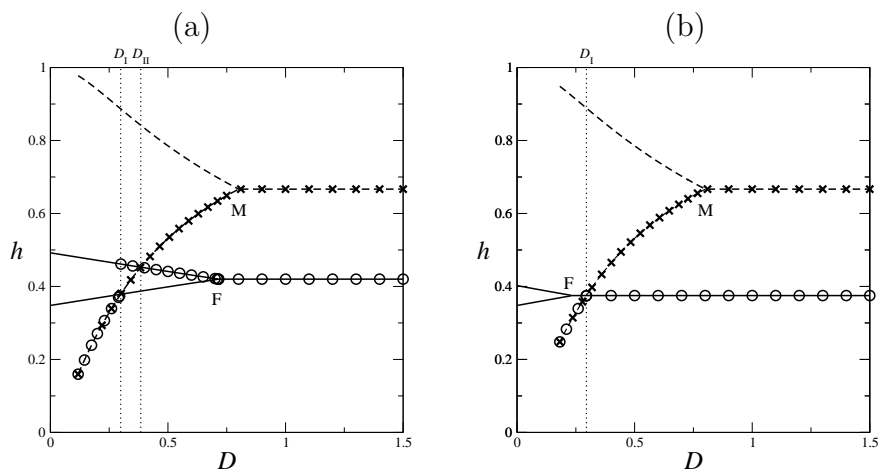


Figure 6: Meniscus and front wedges for (a) Arrangement C, for  $b = 0.16$ , and (b) Arrangement D,  $b = 0.25$ . In Arrangement C,  $D_F < D_M$ , requiring a connection between  $h_B$  and  $(1 - b)/2$  for certain  $D$ . In Arrangement D,  $D_F$  is so small that the front wedge does not intersect  $h_B$  at all.

- A. The most important case is for small  $b$ , i.e., a very thin precursor layer. In this case  $D_F$  is large, and  $h = (1 - b)/2$  is close to its maximum value of  $1/2$ . The upper part of the front wedge  $h_{uc}(D)$  makes intersections with both  $h_T(D)$  and  $h = 2/3$ . This is the arrangement which results when  $b = 0.005$ ; it is shown in Figure 5(a). Here a line marked with circles indicates the left state of the advancing front  $h_f$ , while the right state of the meniscus  $h_m = h_w$  is shown by crosses, for each value of  $D$ . It continues until  $h_{uc}(D_M, b) = 2/3$ ; this happens for  $b = 0.0202$  (4DP).
- B. For larger  $b$ , the line  $h_{uc}(D)$  only makes one intersection with the meniscus wedge, and this is now along the lower branch  $h_B(D)$ . Figure 5(b) shows the situation for  $b = 0.05$ . At  $b = 0.1484$ , the apex of the meniscus wedge and that of the front wedge are at the same value of  $D$ , i.e.,  $D_F = D_M$ .
- C. In the third Arrangement, (for  $0.1484 < b < 0.2338$  to 4 decimal places),  $D_F < D_M$ , but  $h_B(D_F) > (1 - b)/2$ , so the graph of  $h_{uc}(D)$  still intersects  $h_B(D)$ . The significance of this is explained below. Figure 6(a) shows this Arrangement when  $b = 0.16$ .
- D. For the largest  $b$  ( $b > 0.2338$ , to 4 decimal places)  $D_F$  is small enough that the merger at  $D = D_F$  happens with  $h = (1 - b)/2 > h_B(D)$ , i.e., above and to the left of the line  $h_B(D)$  (see Figure 6(b) for  $b = 0.25$ ).

### 3.1 Arrangement A: Thin precursor layer

We begin with the smallest  $D$  (but sufficiently large that  $h_B > b$ ), and argue that the meniscus must be of Type I there. This case applies to values of  $D < D_I$ , where  $D_I$  is where  $h_B = 1 - b - h_{uc}$ , and the lower sides of the two wedges intersect in the  $(D, h)$  diagram. When  $b = 0.005$ , the numerical value for  $D_I = 0.146$ . The other special values of  $D$  given in this section are also for  $b = 0.005$ .

First, suppose the meniscus is of Type II, with a right state thickness  $h_m \geq h_T$ . In this range of  $D$ ,  $h_T$  in turn is larger than  $h_{uc}$ . A connection from  $h_m$  to the precursor would involve a rarefaction fan followed by an undercompressive wave joining to  $b$ . However, the left part of the rarefaction fan would have negative speed, and therefore would fall back into the meniscus. Hence such a solution cannot persist.

On the other hand, if the meniscus is of Type I, then  $h_m = h_B < 1 - b - h_{uc}$ , and a simple compressive connection to the precursor is possible. This is connected by a flat film to a steadily advancing front. The left state of the advancing front and the right state of the meniscus are identical in this case, since the two are directly connected. Our dynamical simulations for  $D = 0.1021 < D_I$  and  $b = 0.005$  (Example 1 of Ref. [11], also shown in Figure 7(a)) confirm that this combination of Type I meniscus and a simple compressive wave occurs. The flat region thickness in this case is controlled by the meniscus.

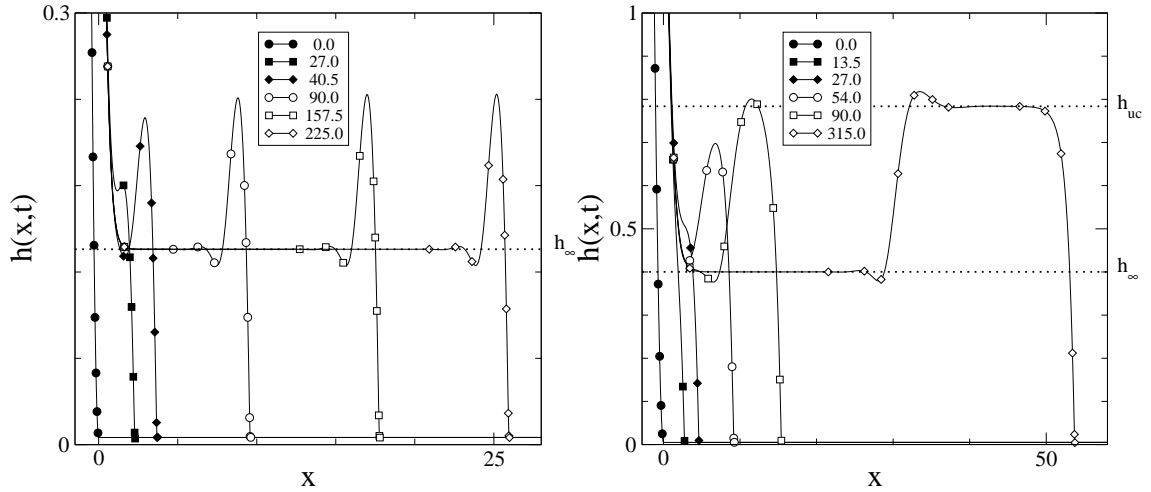


Figure 7: Numerical solutions of (5) when  $D = 0.1021$  ((a), left) and  $D = 0.322$  ((b), right). Film profiles are shown at dimensionless times as given in the legends. In (a), there is a single compressive wave, while in (b), an undercompressive-Lax double shock develops and travels up the substrate. There is a thin precursor film of thickness  $b = 0.005$  in both cases.

When  $D$  is increased above  $D_I$ , the graph of  $h_B(D)$  enters the undercompressive region of the front wedge. In place of a simple compressive connection, a Type I meniscus must now connect to a double shock structure. A Type II meniscus is still not possible, for the same reason as in the previous case, namely that  $h_T > h_{uc}$  while  $D < D_{II}$ . Now the left state of the advancing front is the undercompressive wave height  $h_{uc}$ . The flat region ahead of the meniscus, with thickness  $h_B$ , is connected to  $h_{uc}$  by the trailing compressive part of the double wave structure. This trailing shock moves upwards, but somewhat slower than the advancing front. In the  $(D, h)$  diagram, Figure 5(a), the line marked by circles jumps to  $h_{uc}$  at  $D = D_I$ , separating from the line portion emphasised by crosses.

A complication arises here for those  $D$  where the range of  $h_w$  for which simple compressive waves exists extends to a value  $h'_1$  larger than  $1 - b - h_{uc}$ ; this possibility was highlighted in Section 2.2. Then the meniscus wedge can be connected to either a double shock structure or to a compressive wave. These have a positive wave speed, and which one is selected depends on the initial data. Due to the experience with monotone (jump) initial data, we expect that the simple compressive wave is selected if  $h_B < h'_1$ . The net effect of this is that, for the initial profiles considered in this paper, the transition to the double shock range of  $D$  is delayed and occurs for a value  $D'_I$  slightly larger than  $D_I$ .

This behaviour continues until  $D = D_{II}$ , the value of  $D$  where  $h_{uc} = h_T$  and the upper sides of the two wedges cross. For  $b = 0.005$ ,  $D_{II} = 0.535$ . A double shock structure moving up the substrate is shown for  $D = 0.322$  in Example 2 of Ref. [11], and also in Figure 7(b) just as we described it here.

For  $D_{II} < D < D_{III}$ ,  $h_{uc}$  is larger than  $h_T$  and so it is in the region where Type II

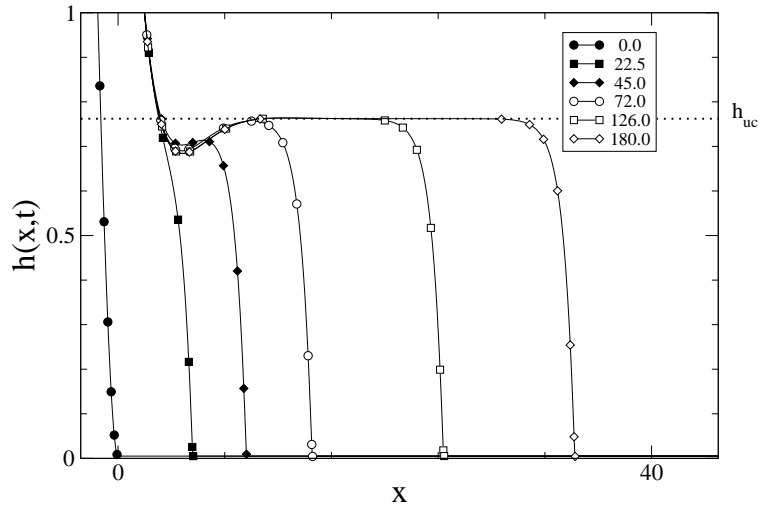


Figure 8: Evolution of (5 for  $D = 0.6424$ , at dimensionless times given in the legends. Only the undercompressive shock propagates away from the meniscus, which evolves into a Type II meniscus. Again the precursor layer thickness is  $b = 0.005$ .

meniscus solutions are possible. Hence a direct undercompressive shock connection from a Type II meniscus to the precursor is possible. (The existence of multiple Type II solutions for  $h$  near  $h_T$  means that a Type II solution is available for matching to  $h_{uc}$  via a direct connection at values of  $D$  slightly below  $D_{II}$ .) These continue until  $D = D_{III}$ , defined by where  $h_{uc} = 2/3$ ; for  $b = 0.005$ ,  $D_{III} = 2.025$ . For  $D < D_{III}$ ,  $h_{uc}$  is larger than  $2/3$ . Thus we can rule out connections involving intermediate waves as follows. Only shocks can connect to  $h_{uc}$  from below, (since characteristics for the left and right state would cross, ruling out a rarefaction fan) and these would have a negative speed. Similarly, any wave connection from above must be a rarefaction fan, all parts of which would also have a negative speed.

As a result, the only structure possible is a Type II meniscus connecting directly to a flat state with thickness  $h_{uc}$ . This flat state is the left state of an undercompressive shock connection to the precursor. The right state of the meniscus and the left state of the advancing front are again identical, and in Figure 5(a) the lines marked by crosses and circles coincide. It is notable that in this range of  $D$ , the thickness of the flat region,  $h_{uc}$ , is determined by the precursor thickness, not by the meniscus. We therefore refer to these structures as “front controlled”. This situation in this range is exactly what is observed for Example 3 from Ref. [11], and in Figure 8, where  $D = 0.6424$ .

Once again, this description has to be slightly amended. The reason is that for  $D < D_B = 0.7142$  Type II menisci exist even for  $h_m$  below  $h_T$ . Hence, in principle, they can arise and connect directly to an advancing front for values slightly smaller than  $D_{II}$ , as an alternative to a double shock structure rising from a Type I meniscus. In this thin region of values of  $D$ , the combination of the wedge diagrams and the criterion for the wave speeds is not sufficient to predict the film behaviour. Instead

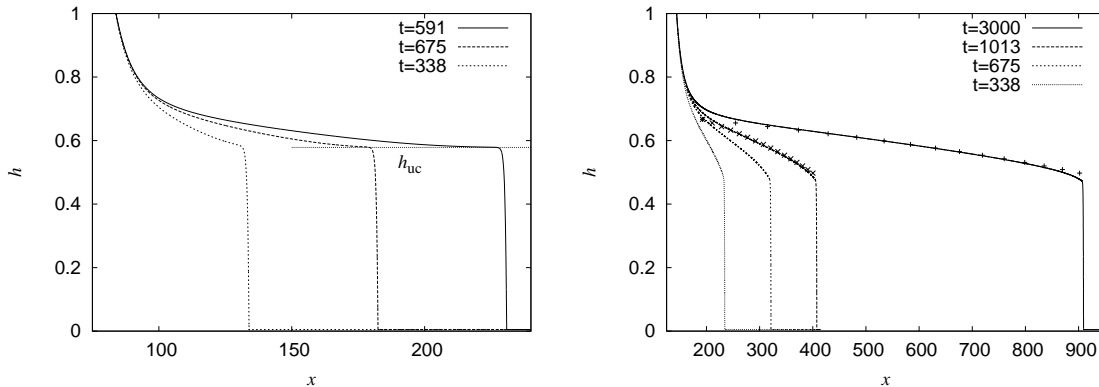


Figure 9: ((a), left) Evolution of (5) when  $D = 3.5$  and  $b = 0.005$ , so  $D < D_F$ . The front is undercompressive. A small flat region of thickness  $h_{uc}$  (indicated by a dotted line) gradually develops behind the front. ((b), right) Evolution of (5) when  $D = 6$  and  $b = 0.005$ . Now  $D > D_F$ , and so the front is a generalised Lax shock. The rarefaction fan is also shown at  $t = 3000$  (+ symbols) and  $t = 1013$  (×); it was obtained by solving the scalar hyperbolic conservation law as described in detail in section 4.

behaviour can be determined by e.g. numerical simulations. We will not elaborate further on this subtlety.

For the small values of  $D$  considered so far, there is in fact a distinct flat region between the meniscus and the wave structure. For larger  $D$ , this is not so. As  $D$  increases beyond  $D_{III}$ , the height of the left state for an undercompressive front  $h_{uc}$  drops below  $h = 2/3$ . Now there can be no direct connection between meniscus and front. All available meniscus profiles have  $h_m$  larger than  $h_{uc}$ , so an intermediate wave is needed to span the gap of thicknesses. From the front wedge part in Figure 2, we see that the resulting wave structure must be a rarefaction-undercompressive wave combination.

No flat film can emerge between the meniscus and the rarefaction wave of thickness  $h_m = h_w$  strictly larger than  $2/3$ , since the portions of the rarefaction wave larger than  $2/3$  would have a negative characteristic speed. Instead the meniscus evolves into a shape that is the limiting profile of all the Type II menisci, while the portions of the film between  $2/3$  and  $h_{uc}$  tend to the profile of rarefaction wave with left state  $2/3$ . Since the characteristic speed at  $h = 2/3$  is exactly zero, the rarefaction wave never completely separates from the meniscus, but as it gets increasingly stretched, the film thickness at a any fixed position  $x$  in front of the meniscus eventually tends to  $2/3$ . We call the emerging limiting meniscus profile with thickness  $h_m = 2/3$  a *generalised Type II meniscus*, in analogy to the terminology for Lax waves.

This situation is indicated in Figure 5(a), where for  $D > D_{III}$ , the crossed and circled lines part again. The former lies at the boundary of the Type II regime, while the latter follows the upper edge of the front wedge. Dynamical simulations with  $D = 3.5$  confirm our picture. In Figure 9(a) we show the evolution of the



film from the initial condition (14), for  $D = 3.5$ . At long times, the film left of the advancing front forms a flat plateau with thickness equal to  $h_{uc} = 0.5783$  (the value was obtained by solving the traveling wave ODE as in [2, 8]). At an increasing distance from the advancing front, the film profile slightly steepens to a rarefaction wave, which blends over into the meniscus.

When  $D$  increases further,  $h_{uc}$  decreases, and the difference between the speed of the undercompressive wave and the left characteristic speed of this wave also decreases. They become equal when  $D = D_F$  and  $h_{uc} = (1 - b)/2$  at the apex of the front wedge. For  $b = 0.005$ ,  $D_F = 5.227$ . For the largest  $D$ , in excess of  $D_F$ , the possible wave structures are those that are permitted according to classical shock theory.

Again, the meniscus profile tends to a generalised Type II meniscus, and it must connect to a rarefaction fan with left state  $2/3$ . The rarefaction wave now connects directly to the advancing front, which connects in turn to  $b$ . The characteristic speed of the thickness  $(1 - b)/2$  where the two structures connect is identical to the shock speed. The leading shock is therefore a generalized Lax wave, which is not undercompressive, and there is neither the flat region of thickness  $h_{uc}$  nor the steep shock front which were visible when  $D = 3.5$ . This is seen in a dynamical simulation for  $D = 6$  in Figure 9(b). Instead the rarefaction fan expands over time, always stretching from the meniscus to the advancing front. The front is a generalized Lax shock, and connects to the rarefaction fan via a rounded corner at thickness  $h = (1 - b)/2 = 0.4975$ .

### 3.2 Arrangement B: thicker precursor layer, $0.0202 < b < 0.1484$

For larger precursor thicknesses, the expected film configuration is generally similar to the small  $b$  case described above. However some new configurations do appear for a range of  $D$  values, while the front-controlled profiles with a Type II meniscus and flat region thicker than  $2/3$  no longer occur.

The intersections occurring at  $D = D_{II}$  and  $D = D_{III}$  both happen at  $D = D_M$  when  $b = 0.0202$ . For larger  $b$ , the upper branch  $h_{uc}$  of the front wedge intersects only the lower branch of the meniscus wedge. We call the value of  $D$  for the remaining intersection  $D_{II}$ . The two wedges are shown for  $b = 0.05$  in Figure 5(b). We describe the profiles which result as  $D$  is increased below.

For  $D < D_{II}$ , the film behaves as for the first two cases in Arrangement A (Section 3.1). For the smallest  $D$ , profiles continue to be controlled by the meniscus, with a Type I meniscus, a flat region of thickness  $h_B$ , and simple compressive front, with a capillary ridge connecting the flat region to the precursor layer. When  $D_I < D < D_{II}$ , there is again a Type I meniscus, and flat region with thickness  $h_B$ , but at the advancing front, there is a double shock structure. Both these behaviours have been seen in our dynamic simulations with  $b = 0.05$ .

Because  $h_{uc}(D)$  is smaller than in Arrangement A for the larger values of  $b$  considered

here, it never exceeds  $h_T$ , the threshold for a Type II meniscus. (See Figure 5(b).) Thus for this range of  $b$ , there are no front-controlled profiles. Instead, for  $D_{\text{II}} < D < D_M$ , a new configuration is possible. Now both  $h_B$  and  $h_T$  are greater than  $h_{\text{uc}}$ , so any connection from the meniscus must be via a rarefaction fan. This cannot connect to a Type II meniscus, since  $h_T > 2/3$  and so the left part of the rarefaction would have negative speed. So here there is a Type I meniscus, connected via a rarefaction fan to a flat region of height  $h_{\text{uc}}$  where the film is thinner. This in turn is connected via an undercompressive shock to  $b$ . All parts of the rarefaction wave have positive speed, but the undercompressive wave is faster than the leading edge of the rarefaction fan, so the length of the flat region between the meniscus increases with time. Dynamical simulations with  $D = 0.7$  and  $b = 0.05$ , shown in Figure 10(a), confirm that two flat regions develop. The first has thickness close to  $h_B = 0.6298$ , as expected for a Type I meniscus solution for this value of  $D$ , and extends up to the rarefaction fan. A second develops between the rarefaction fan and the advancing front, with a thickness close to the expected undercompressive region height  $h_{\text{uc}} = 0.5907$ .

For  $D > D_M$ , the behaviour is similar to that for  $D > D_{\text{III}}$  for small  $b$  (Section 3.1). There is a rarefaction fan extending from a generalised Type II meniscus at  $h = 2/3$  to  $h_{\text{uc}}$ . Provided that  $D < D_F$ , a flat region of thickness  $h_{\text{uc}}$  exists before an undercompressive shock, while for  $D > D_F$  there is no flat region, and the connection to the precursor is a generalised Lax shock.

### 3.3 Arrangement C: yet thicker precursor layer, $0.1484 < b < 0.2338$

As  $b$  is further increased,  $D_F$  reduces, so that when it reaches the critical value  $b = 0.1484$ ,  $D_F$  and  $D_M$  are equal. For somewhat larger  $b$  (so that  $D_F < D_M$ , but is not too small) the apex of the front wedge still lies outside the meniscus wedge. This arrangement of the wedges is shown in Figure 6(a) when  $b = 0.16$ .

In this arrangement, the film behaves as for Arrangements A and B while  $D < D_{\text{II}}$ , forming a Type I meniscus with compressive shock for  $D < D_{\text{I}}$ , and then a double shock for  $D_{\text{I}} < D < D_{\text{II}}$ . For  $D > D_{\text{II}}$ , but less than  $D_F$ , the Type I meniscus still exists, and connects to the precursor via a flat region of thickness  $h_B$ , then a rarefaction fan and undercompressive shock as in Arrangement B. In dynamic simulations the flat  $h_{\text{uc}}$  region takes a long time to develop.

For  $D_F < D < D_M$  another new behaviour occurs. Type I menisci are still possible, but they must connect to the precursor by a rarefaction fan with right state  $(1-b)/2$ , followed by a classical generalised Lax shock, since undercompressive connections do not exist for  $D > D_F$ . Such behaviour is seen in Figure 10(b), for  $D = 0.72$  and  $b = 0.16$ . (Note that  $D_F = 0.7153$  for  $b = 0.16$ .) Here  $h_B = 0.6376$ , and it is apparent that in the meniscus region the film approaches this thickness before entering the rarefaction fan region and dropping to  $(1-b)/2 = 0.42$ . Since  $h_B$  is quite close to  $2/3$  here, characteristics have a slow speed, and the left edge of

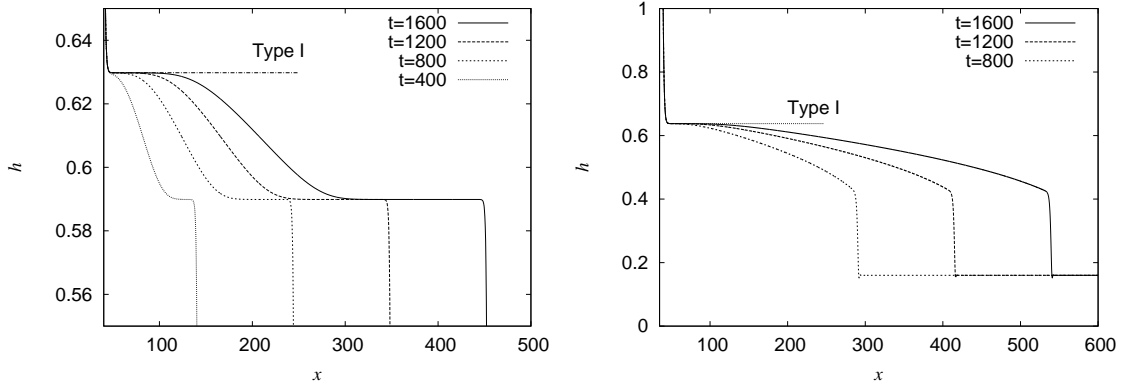


Figure 10: ((a), left) Evolution of the film when  $D = 0.7$  and  $b = 0.05$  (so  $D_{II} < D < D_M$ ). A Type I meniscus, which tends towards  $h_B = 0.6298$ , is connected via a rarefaction fan to a flat region of height  $h_{uc}$  which connects to the precursor thickness  $b$  via an undercompressive shock. This configuration is only possible when  $b > 0.0202$ . ((b), right) Evolution of the film when  $D = 0.72$ . Here  $b = 0.16$ . The front is now a generalised Lax wave, unlike that seen in the left figure. The meniscus is still Type I, approaching a value  $h_B = 0.6376 < 2/3$ . A knee develops close to  $h = (1 - b)/2 = 0.42$ .

the rarefaction fan takes a long time to move away from the meniscus. Finally, for  $D > D_M$ , behaviour is again as for the largest  $D$  values in Arrangements A and B: a generalised Type II meniscus connects to a rarefaction fan and from there to a generalised Lax wave, as in Figure 9(b).

### 3.4 Arrangement D: thickest precursor layers: $b > 0.2338$

In this arrangement,  $D_F < D_I$  and the front wedge lies entirely within the meniscus wedge. Figure 6(b) shows the case  $b = 0.25$ . Three types of behaviour are possible; these are similar to those of Arrangement C.

For small  $D < D_I$  (but sufficiently large that  $h_B > b$ ), the film continues to display meniscus-controlled behaviour. There is a Type I meniscus, followed by a flat region with thickness  $h_B(D)$  which is connected to the precursor layer by an compressive advancing front. This is the case regardless of whether  $D$  is larger or smaller than  $D_F$ .

When  $D > D_I$ , the connection to the precursor must be via a classical structure (since  $D_I > D_F$ ). Since the preferred right state of the meniscus exceeds  $(1 - b)/2$ , there is a rarefaction fan, connecting to a classical generalised Lax shock. The two behaviours possible for  $D > D_I$  differ near the meniscus: for  $D_I < D < D_M$ , it is a Type I meniscus which connects to the rarefaction fan as in Section 3.3. Once  $D$  exceeds  $D_M$ , there is a generalised Type II meniscus that joins to the rarefaction fan, as for the largest  $D$  values in the previous arrangements.

## 4 Nearly-horizontal substrate: large $D$

For a substrate which is nearly horizontal, the levelling effects of the normal component of gravity become important. Here we consider steady state profiles in the limit  $D \rightarrow \infty$ . For studying this regime, we adopt a scaling in which surface tension is neglected, but both components of gravity are retained. Smoothing of discontinuities in the film is now provided by the normal component of gravity instead of predominantly by surface tension. Rescaling by defining  $\tilde{x}$  and  $\tilde{t}$  by

$$D\tilde{x} = x \quad D\tilde{t} = t, \quad (6)$$

and letting  $D \rightarrow \infty$  causes the governing PDE (5) to reduce from fourth to second order:

$$h_{\tilde{t}} + \left(h^2 - h^3\right)_{\tilde{x}} = \left(h^3 h_{\tilde{x}}\right)_{\tilde{x}}. \quad (7)$$

Steady-state solutions of (7) which represent feasible meniscus profiles must satisfy boundary conditions far upstream and downstream. The film must match onto the reservoir, so

$$\frac{dh}{d\tilde{x}} \rightarrow -1 \quad \text{as } \tilde{x} \rightarrow -\infty,$$

(which is simply the rescaled form of (3)) and its thickness must approach a constant value  $h_m$  far downstream:

$$h \rightarrow h_m \quad \text{as } \tilde{x} \rightarrow \infty.$$

Setting  $h_{\tilde{t}}$  to zero, Equation (7) can be integrated with respect to  $\tilde{x}$  to yield a first-order (nonlinear) ODE:

$$h_{\tilde{x}} = \frac{h^2 - h^3 - c}{h^3} \quad (8)$$

For large  $h$ , Equation (8) has  $h_{\tilde{x}} \rightarrow -1$ , and by setting the constant of integration  $c = (h_m^2 - h_m^3)$ , both boundary conditions are satisfied. Note that  $c$  is the total flux of liquid flowing through the flat film in front of the meniscus; physically meaningful values for climbing films are  $0 < c \leq 4/27$ . A one-parameter family of solutions is generated by varying  $h_m$ , or alternatively,  $c$ . For  $c < 4/27$ , the positive-valued fixed points of Equation (8) are  $h = h_B < 2/3$  and  $h = h_T > 2/3$ , the same as those of the steady form of Equation (5).

When  $h_B$  and  $h_T$  are distinct, Equation (8) shows that  $h_{\tilde{x}}$  is negative for  $h > h_T$  and  $h < h_B$ , and positive for  $h_B < h < h_T$ ;  $h_T$  is therefore a stable fixed point while  $h_B$  is unstable. Any solution which becomes infinite as  $\tilde{x} \rightarrow -\infty$  must be monotonic, decreasing, and have  $h > h_T > 2/3$  everywhere, with  $h \rightarrow h_T$  as  $\tilde{x} \rightarrow \infty$ . In other words, the meniscus profiles for  $c < 4/27$  connect to a thickness  $h_m > 2/3$ , and so are Type II profiles. The exact solution to (8), up to translation in  $\tilde{x}$ , is given implicitly by

$$\tilde{x} = -h + \sum_{i=1}^3 \frac{h_i^3}{(h_i - h_j)(h_k - h_i)} \log |h - h_i| \quad (9)$$

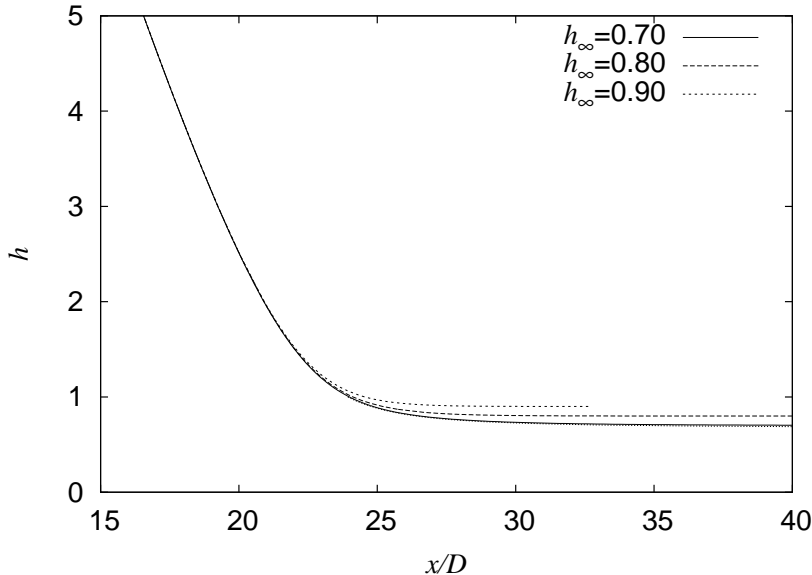


Figure 11: Solutions of Equation (8), in a parameter regime where surface tension is unimportant. Shown are  $h_m = 0.7, 0.8, 0.9$ . On this scale, the solution with  $h_m = 0.7$  is barely distinguishable from the solution of (10) with  $h_m = 2/3$ , shown as a dotted line.

where the summation is over the three distinct roots  $h_B$ ,  $h_T$ , and  $(1 - h_B - h_T)$  of the cubic equation  $h^2 - h^3 - c = 0$ . Solutions of the form of (9) are shown in Figure 11 for three values of  $h_m > 2/3$ . The solution with  $h_m = 0.91$  is compared to meniscus profiles with finite  $D$  in Figure 12. As the influence of surface tension diminishes, the dip disappears, and the meniscus profiles become monotone, even though they are of Type II.

As  $h_m$  approaches  $2/3$ , the fixed points  $h_B$  and  $h_T$  also approach  $2/3$ . When  $h_m = 2/3$ ,  $c = 4/27$ , and there is a repeated root of  $h^2 - h^3 - c = 0$ . The solution to (8) is then given by

$$\tilde{x} = -h + \frac{8}{27} \frac{1}{h - 2/3} - \frac{28}{27} \log \left| h - \frac{2}{3} \right| + \frac{1}{27} \log \left| h + \frac{1}{3} \right| \quad (10)$$

The  $(h - 2/3)^{-1}$  term rapidly blows up, indicating that the film requires a very long distance to reach its limiting value  $h_m$ . The solution for  $h_m = 2/3$  is shown in Figure 11 as a dotted line.

At this point, we have established essentially the same picture for the possible meniscus structure as for the large (but finite)  $D$  case discussed in Section 3. On the other hand, since Equation (7) is a second order equation, the classical theory of shocks only allows a rarefaction fan and generalised Lax shock combination for connecting a thickness larger than  $(1-b)/2$  with a precursor of thickness  $b$ . Therefore in numerical simulations of (7), a generalised Type II meniscus profile should emerge connected to such a combination and indeed, this is seen in the results of the previous section for sufficiently large  $D$ .

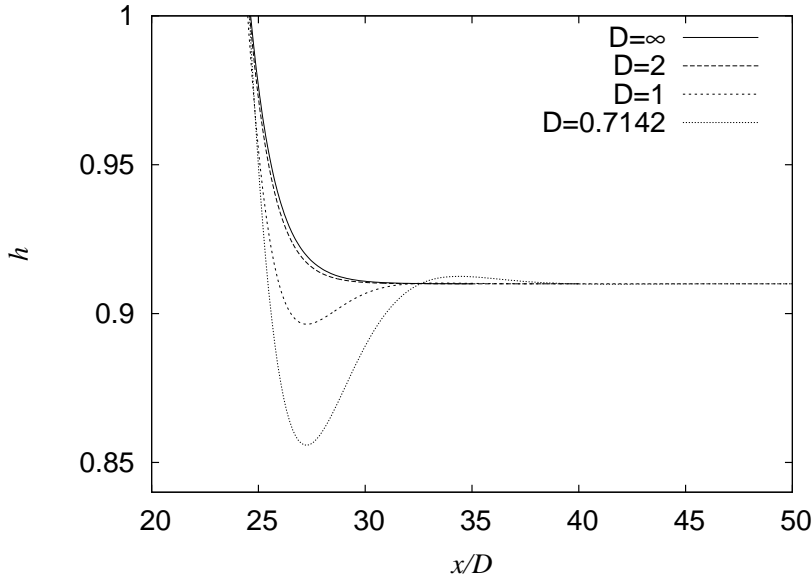


Figure 12: Steady solutions of (5) which have  $h_m = 0.91$ , rescaled according to (6). As  $D$  is increased, these approach the large  $D$  limit, shown as a solid line. The dip which is a feature of Type II solutions for small  $D$  is gone for  $D = 2$ .

We compared the profiles obtained from our dynamic model including the surface tension terms (5) for two moderately large values of  $D$  with those of the time-dependent model (7) valid when  $D \rightarrow \infty$ . Simulations were performed with  $b = 0.005$ , for which  $D_F \approx 5.227$ . The same initial condition (14, given in the Appendix) was used for each case.

As described in Section 2.2, when  $D$  is larger than  $D_F$ , the presence of the surface tension terms are expected to give rise to a classical front, with a rarefaction fan connected to a compressive shock. Numerical simulations with  $D = 6$  confirm this. This is shown in Figure 9(b), where the front advances with a rounded corner, typical of a generalised Lax shock. In contrast, when  $D = 3.5 < D_F$  the advancing front is undercompressive (Figure 9(a)). It separates from the rarefaction wave and has a markedly higher left state. At the same rescaled time  $\tilde{t} = 169$ , the rescaled profiles for the meniscus region and much of the film are very similar to the large  $D$  result, i.e., using (7), for both finite  $D$  values. This is shown in Figure 13. However at the advancing front, the difference between the undercompressive and generalised Lax fronts is evident, while the transition from generalised Lax wave to the precursor is slightly more rounded for  $D = 6$  than for  $D = \infty$ .

Finally, we demonstrate that the portion behind the advancing front seen in Figure 9(b) (and also Figure 10(b)) is indeed a rarefaction fan, by comparing it directly to solutions of the first order equation resulting from neglecting all second- and fourth-order smoothing terms in (5). Rarefaction wave solutions of  $h_t + f(h)_x = 0$ , may be found, subject to appropriate initial data, using the method of characteristics. Thus within the rarefaction fan delimited by left and right states  $h_-$  and

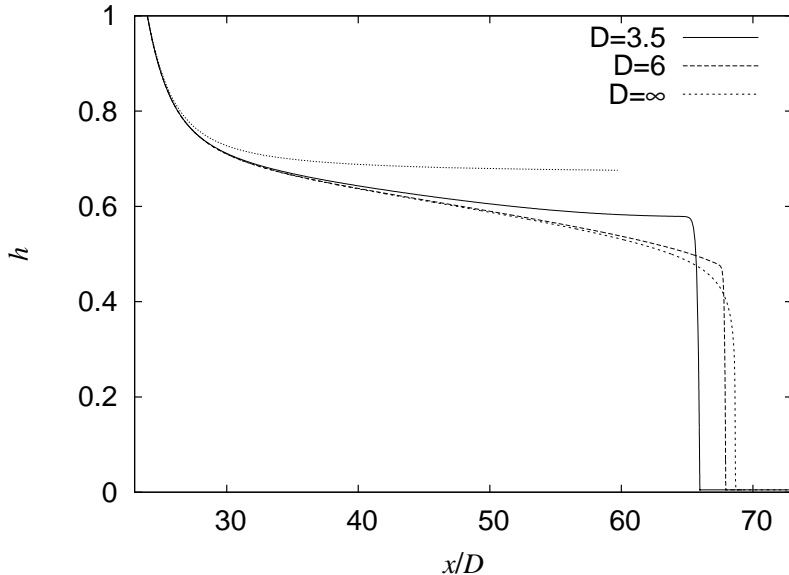


Figure 13: Advancing fronts with  $b = 0.005$ , and different  $D$ , shown at the same scaled time  $\tilde{t} = 169$ . Also shown is the long-time solution for  $h_m = 2/3$  and  $D = \infty$  (dotted line), which is approached by the solutions for large  $D$ , and when the front has moved far from the meniscus.

$h_+$ ,

$$h(x, t) = h_R(\xi) = (f')^{-1}(\xi), \quad \text{where } \xi = \frac{x - x_0}{t - t_0} \quad (11)$$

for some  $x_0$  and  $t_0$ . The function  $h_R(\xi)$  is given implicitly by  $\xi = f'(h) = 2h - 3h^2$ . The unknowns  $x_0$  and  $t_0$  may be estimated as follows. For the situation shown in Figure 9(b), we take  $h_+$  to be  $(1-b)/2 = 0.4975$ . At a given time,  $t_2$  say, we observe where  $h(x, t_2) = h_+$ , at  $x = x_+$  say, and estimate a value for  $t_0$ . We then compute

$$x_0 = x_+ + (t_2 - t_0)\xi_+$$

where  $\xi_+ = f'(h_+)$ . The shape of the rarefaction fan may be constructed at any time  $t$  using

$$x = (t - t_0)\xi(h) + x_0 \quad \text{for } h_+ < h < 2/3 \quad (12)$$

We vary  $t_0$  until (12) provides a good fit for  $h(x, t_2)$  within the rarefaction fan.

We demonstrate this by computing the rarefaction fan constants  $x_0$  and  $t_0$  using our result at  $t = 3000$  (shown using “+” symbols in Figure 9(b)) and then confirming these by comparison with (12) at  $t = 1013$  (“×” symbols in Figure 9(b)). The agreement is satisfactory in the interior of the rarefaction fan. At the ends, the higher-order terms in (5) are important and smooth the profile.

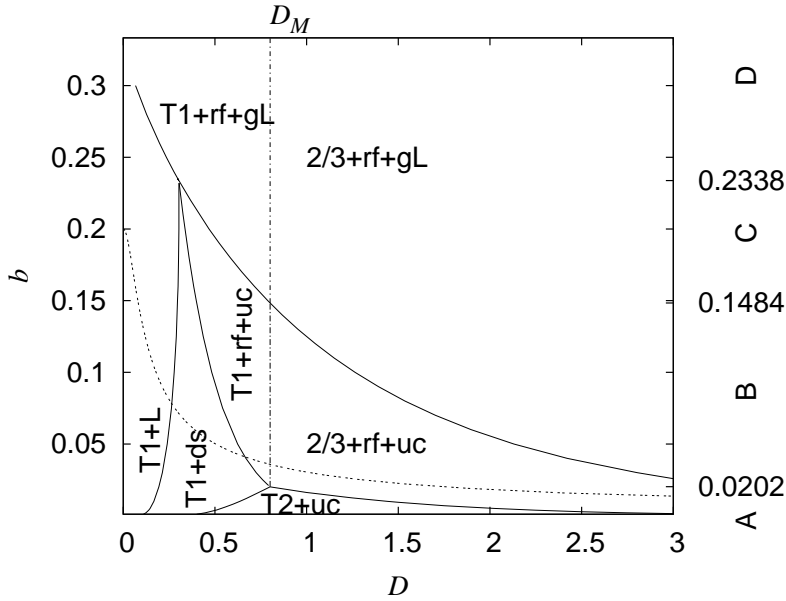


Figure 14: Behavior of a thin surface-tension-gradient-driven film emerging from a meniscus. The thickness  $b$  of a thin precursor layer, and an inclination parameter  $D$  control the behaviour. The following abbreviations are used, and explained in the text: T1, T2 and 2/3 denote Type I, Type II and 2/3 (generalised Type II) menisci respectively; the other labels are: L — (compressive) Lax wave; ds — double shock gL — generalised Lax wave; rf — rarefaction fan; uc — undercompressive shock. The dotted line indicates points which differ only in tilt angle  $\alpha$ .

## 5 Summary of behaviour: a catalogue

The previous sections’ observations can be summarised by considering regions of  $(D, b)$  parameter space in which distinct behaviours arise. These are shown in Figure 14. The lines  $D_i(b)$  ( $i = \text{I, II, III}$ ) and  $D_F(b)$  divide the parameter space into several regions. These regions are indicated by the labels in the figure. The descriptions of the Arrangements described in Section 3 correspond to moving along horizontal lines (constant  $b$ ) in this figure.

A number of features are apparent. For small  $D$  (though with  $D \gg \epsilon$ ), a Type I meniscus (labelled “T1+L”) results for all choices of  $b$ . At the other extreme, for the largest  $D > \max(D_F, D_M)$ , the advancing front is a generalised Lax wave, and the connection to the meniscus is via a rarefaction fan (labelled “2/3+rf+gL”). States in which there is a distinct separation and flat region between the meniscus and front—the Type I meniscus with a Lax front, and the Type II meniscus, with a double shock structure or undercompressive front—exist only in the lower left part of the diagram, shown by labels “T1+L”, “T1+ds” and “T2+uc”. These are states are familiar from previous work e.g. [11]. For a fixed value of  $D$ , one of these separated configurations can only arise when a sufficiently thin precursor is present. As the precursor layer is thickened these give way to film profiles with rarefaction fans,



shown by “rf” in the figure labels. These new kinds of behaviour were described in Section 3. In particular, the combination of a Type I meniscus and rarefaction fan seen in Figure 10(a) only occurs for  $b > 0.0202$ , while a Type II meniscus with an extended flat region and undercompressive front only occurs for  $b$  smaller than this value. In the upper-right part of the diagram lie structures with rarefaction fans, for which there is no clear separation between the meniscus and the front.

It should be noted that in a set of experiments, the dimensional precursor thickness  $b^*$  (or equivalently the wetting behaviour) is likely to be fixed. If the substrate angle  $\alpha$  is varied while other parameters including  $b^*$  are fixed, then this corresponds to moving along a curved path in Figure 14, given parametrically by  $((3\delta)^{2/3} \sin \alpha / \cos^{4/3} \alpha, b_0 \cos \alpha)$  where  $b_0$  is the dimensionless precursor thickness for  $\alpha = 0$ . One such curve is shown in the figure for  $\delta = 0.00782$ , corresponding to experiments by Schneemilch and Cazabat [12], and  $b_0 = 0.2$ , as a dotted line. This value is likely to be larger than in their experiments, but demonstrates how the film changes, from a Type I meniscus and compressive front to more complex behaviour, as  $\alpha$  is increased. For this value of  $\delta$ , values of  $b_0 > 0.11$  result in not entering the “T2+uc” region for any  $\alpha$ .

## 6 Concluding remarks

In this paper, understanding of the film on a heated tilted substrate near a meniscus and at an advancing front has been combined to generate an understanding of the possible behaviour for the entire film. This is graphically summarised by Figure 14. This analysis is based on approximating the curvature, which is appropriate for relatively tilted substrates. In practice, angles of more than  $45^\circ$  should be sufficient for the theory here to apply. For example, when  $\delta = 0.00782$ , taking  $\alpha > 56^\circ$  is sufficient to ensure  $\epsilon < 0.1$ .

When  $D$  is of order  $\epsilon$  or smaller, the curvature can no longer be approximated by  $h_{xx}$  everywhere. In this limit  $h_B$  approaches a finite non-zero value [3, 4, 9, 11]. For practical values of the shear stress, the most significant effect is to move the bottom edge of the meniscus wedge so that the graph of  $1 - b - h_{uc}$  no longer intersects  $h_B(D)$ . This situation occurs more easily for smaller values of  $b$ . In that case, instead of a Type I meniscus with a compressive front for the smallest values of  $D$ , either a double shock profile or a Type II meniscus with undercompressive front may occur. In principle, this means that undercompressive advancing fronts are possible for nearly-vertical substrates provided that the precursor layer is sufficiently thin.

Our results indicate that when the control parameter  $D$  is sufficiently large there is no extended flat region, but rather a rarefaction fan links the meniscus to the advancing front. An interesting observation is that when a Type II meniscus arises, its flat region thickness is not controlled by conditions at the meniscus, as for the Type I meniscus; instead it is the precursor thickness which determines  $h_{uc}$  and so the thickness of the flat region.

Similarly the interesting question of what would happen if the film were to advance over a substrate for which wetting is imperfect, i.e., for which there is a non-zero contact angle, has not been addressed. For the drag-out problem, there is a minimum withdrawal speed required to draw out a film, if the contact angle is prescribed [6].

Despite these limitations, we expect that the guide presented here will be a useful tool for experimentalists. We look forward to experimental confirmation of the results here.

## Acknowledgements

Supported by the DFG Research Centre MATHEON (Project C10) in Berlin. AM was also supported by a Heisenberg Fellowship.

## A Numerical details

To obtain numerical solutions of (5), and (7) we used finite difference schemes on a finite spatial domain,  $[0, L]$ . At the left-hand boundary, we specify  $h = H_0$  to be a large constant (typically 20–50) and impose  $h_{xxx} = 0$ . At the right-hand boundary,  $h_x = h_{xxx} = 0$ . Solutions are advanced in time using an implicit Euler scheme. The time step was controlled using a step-doubling approach.

Simulations began from an initial profile  $h(x, 0) = h_0(x)$ . The form used for  $h_0$  was generally

$$h_0(x) = \begin{cases} D^{-3/2} (\exp(D^{1/2}x) - D^{1/2}x - 1) + b & \text{for } x \leq 0, \\ b & \text{for } x > 0. \end{cases} \quad (13)$$

This represents the static meniscus which arises through the balance of mean surface tension and gravity for  $x < 0$ , and joins smoothly to the precursor layer at  $x = 0$ . Other initial profiles, including the function

$$h_0(x) = \frac{\log(2 \cosh(ay)) - ay}{2a} + b \quad (14)$$

where  $y = x/D - 20$  and  $a = 0.4$ , were also used. This has slope  $-1$  for  $x \rightarrow -\infty$ , and  $\rightarrow b$  as  $x \rightarrow \infty$ . We also used

$$h_0(x) = \max(-x/D, b) .$$

The particular choice did not alter the qualitative behaviour of the film.

## References

- [1] A. L. Bertozzi, A. Münch, X. Fanton, and A. M. Cazabat. Contact line stability and ‘undercompressive shocks’ in driven thin film flow. *Phys. Rev. Lett.*, 81(23):5169–5172, December 1998.

- [2] A. L. Bertozzi, A. Münch, and Michael Shearer. Undercompressive waves in driven thin film flow. *Physica D*, 134:431–464, 1999.
- [3] Phillippe Carles and Anne-Marie Cazabat. The thickness of surface-tension-gradient-driven spreading films. *Journal of Colloid and Interface Science*, 157:196–201, 1993.
- [4] X. Fanton, A. M. Cazabat, and D. Quéré. Thickness and shape of films driven by a Marangoni flow. *Langmuir*, 12(24):5875–5880, 1996.
- [5] Ryan P. Haskett, Thomas P. Witelski, and Jeanman Sur. Localized Marangoni forcing in driven thin films. *Physica D*, 2005. Accepted.
- [6] L. M. Hocking. Meniscus draw-up and draining. *European Journal of Applied Mathematics*, 12:195–208, 2001.
- [7] O. K. Matar and R. V. Craster. Models for Marangoni drying. *Physics of Fluids*, 13(7):1869–1883, July 2001.
- [8] Andreas Münch. Shock transitions in Marangoni-gravity driven thin film flow. *Nonlinearity*, 13:731–746, 2000.
- [9] Andreas Münch. The thickness of a Marangoni-driven thin liquid film emerging from a meniscus. *SIAM Journal on Applied Mathematics*, 62(6):2045–2063, 2002.
- [10] Andreas Münch. Pinch-off transition in Marangoni-driven thin films. *Physical Review Letters*, 91(1):id: 016105, 2003.
- [11] Andreas Münch and P. L. Evans. Marangoni-driven liquid films rising out of a meniscus onto a nearly horizontal substrate. *Physica D*, 2005. Accepted.
- [12] M. Schneemilch and A. M. Cazabat. Shock separation in wetting films driven by thermal gradients. *Langmuir*, 16:9850–9856, 2000.
- [13] M. Schneemilch and A. M. Cazabat. Wetting films in thermal gradients. *Langmuir*, 16:8796–8801, 2000.
- [14] Leonard W. Schwartz. On the asymptotic analysis of surface-stress-driven thin-layer flow. *Journal of Engineering Mathematics*, 39:171–188, 2001.